



Original Article

Effect of Aortic Wall Deformation with Healthy and Calcified Annulus on Hemodynamic Performance of Implanted On-X Valve

MASOD SADIPOUR, PEDRAM HANAFIZADEH , KEYVAN SADEGHY, and AMIRMOHAMMAD SATTARI

School of Mechanical Engineering, College of Engineering, University of Tehran, Tehran, Iran

(Received 10 September 2019; accepted 24 December 2019; published online 7 January 2020)

Associate Editors Francesco Migliavacca, Ajit Yoganathan oversaw the review of this article.

Abstract

Introduction—In this research, the hemodynamic performance of a 23-mm On-X bileaflet mechanical heart valve (BMHV) was investigated with the realistic geometry model of the valve and the deformable aorta in accelerating systole. In addition, the effect of ascending aorta flexibility and aortic annulus calcification on the complex blood flow characteristics were investigated.

Methods—The geometry of the aorta is derived from the medical images, and the Ogden model has been utilized for the mechanical behavior of the ascending aorta. The 3D numerical simulation by a two-way Fluid-Structure Interaction (FSI) analysis using the Arbitrary Lagrangian–Eulerian (ALE) method was performed throughout the accelerating systolic phase.

Results—The dynamics of the leaflets are investigated, and blood flow characteristics such as velocities, vorticities as well as viscous and turbulent shear stress were precisely captured in the flow domain specifically in the hinge region. Streamline results are in accordance with the previously reported data, which show that the flared On-X valves inlet yields a more uniform flow in accelerating systole. Simulations show that aorta flexibility or valve annulus calcification causes variations up to 7% in maximum fluid velocity and 20% in Turbulence Kinetic Energy (TKE).

Conclusions—In this study, the complex flow field characteristics in the new generation of BMHVs considering aorta flexibility with healthy and calcified annulus were investigated. It was found that the blood flow around the hinges region is in the danger of hemolysis and platelet activation and subsequently thromboembolism. Furthermore, the results show that similar to vessel wall deformation, consid-

ering the probable annulus calcification after valve replacement is also essential.

Keywords—Bileaflet mechanical heart valve, Numerical simulation, Hemodynamic performance, Flexible vessel wall, Calcified aortic annulus.

INTRODUCTION

Valvular heart illness is affecting more than 100 million people globally, and in some severe cases, can cause a significant mortality rate.¹ Nowadays, many patients all over the world suffer from heart diseases, and the number of patients increases as the average age of the population increases.^{1,40,41} Valve calcification, stiffening the valve, Rheumatic fever, and bicuspid valve are the most typical problems associated with the aortic valve. These problems can be solved by repairing the valves or replacing the diseased valves with artificial valves.^{26,37} Mechanical heart valves (MHVs) are the most acceptable prostheses valves that are utilized due to their lifelong durability.^{1,40} The main disadvantage of MHVs is the need for long-term anticoagulant medicine, which limits its clinical application.⁶ Nowadays, among the mechanical heart valves, surgeons usually use the BMHVs.⁴¹

However, there are still some problems in BMHVs such as thrombosis, cavitation, backflow, *etc.* These problems are related to the non-physiological pattern of blood flow that leads to the mechanically induced damage of blood cells.¹⁶ Numerical simulation can serve as a tool to not only infer reliable prosthesis function but also to consider and facilitate the design of future prosthetic valves.⁴² In this respect, CFD analysis can be used to investigate the behavior of the

Address correspondence to Pedram Hanafizadeh, School of Mechanical Engineering, College of Engineering, University of Tehran, Tehran, Iran. Electronic mail: Masod.sadipour@ut.ac.ir, Hanafizadeh@ut.ac.ir, Sadeghi@ut.ac.ir, Amirsattari@ut.ac.ir

blood flow passing through the BMHVs. Earlier studies in this regard were conducted to investigate the angle of leaflets and hemodynamic performance of BMHVs in the cardiac cycle at a particular time point with static 2D geometry. One of the earlier researches is done by King *et al.*²⁴ in which they performed a 2D steady-state simulation of bileaflet mechanical heart valve utilizing CFD. They investigated the effect of flow pattern with non-Newtonian blood flow and compared it with 3D experimental results. They found that 2D simulation has a significant difference in flow distribution with experimental results. The CarboMedics and St. Jude heart valves prosthesis were subsequently compared, and it was detected that the St-Jude valves demonstrated fewer disturbances due to their larger opening angle. Afterward, in another research done by King *et al.*,²³ a 3D precise transient simulation was conducted, and the velocity profile in different places was investigated and compared with the experimental data. They found that the flow field shows an appropriate correspondence with the experimental data, and at the opening angle, the location of the leaflet also influences the disturbances. Moreover, they concluded that CFD is a powerful tool to predict the fluid flow in the downstream of the mechanical heart valve. In order to investigate the vortexes, which are among the critical issues that lead to thrombosis, Bluestein *et al.*⁷ performed a 2D transient simulation of BMHV that the leaflets are fixed in a fully open location by utilizing $k - \omega$ as the turbulence model. They introduced diffusion of vortexes as a mechanism for activating platelets. They stated that non-tissue surfaces of the mechanical valves cause a non-physiological flow pattern, which is one of the notable limitations of mechanical valves. Consequently, in their work, vortexes were the leading cause of the production of free clots.

After the examination of leaflets angle and main characteristics in the fluid with fixed leaflets, the research interest in this subject shifted towards studying the movement of leaflets. The fluid-solid interaction simulation of blood flow in BMHVs was studied by Cheng *et al.*,⁹ in which simulation was performed only on one-quarter of the fluid field in the diastolic phase. They stated that Wall Shear Stress (WSS) from blade motion is the main reason for the coagulation; consequently, they examined the flow near the leaflets in the diastolic phase. They reported that high velocities in the small distance between the leaflet and housing wall during the leaflet return as well as leaflets collision to the blood, leading to high WSS. In another research, the fluid-solid interaction simulation in a 2D simplified model was conducted by Dumont *et al.*¹³ They validated the results of numerical data against the experimental one. It was observed that FSI simu-

lation with dynamic mesh could predict the exact motion of leaflets. After validation of the method, in another study, they¹⁴ compared the hemodynamic performances of St. Jude, and ATS open pivot in a not only 3D simulation with exact geometry but also with the transient condition. They stated that these two valves mainly differ in their hinge design, and exhibit two different characteristics in the activation of platelets. Their findings indicate that, in the closure phase, the St. Jude valve is more prone to platelet activation than the ATS open pivot. Ge *et al.*¹⁷ examined the effectiveness of various turbulence models in stimulating the characteristics of BMHVs. They showed that by moving to the flow downstream, the vortexes generated near the wall increase their distances from the wall and compress the central jet, and consequently, the flow is divided into two jets. It was also claimed that the Detached Eddy Simulation method is a reliable tool in modeling turbulent flow.

As critical characteristics of the blood flow are mostly rooted in regions like sinuses or hinge areas, there are some studies focused on the blood flow in these regions. Bang *et al.*⁵ studied the effect of sinuses existence in the aorta model geometry on the flow field in two kinds of vessels: with and without sinuses. In this simulation, they utilized FSI analyses for curved BMHV. Their results showed that the model without sinuses takes more time in the closure phase. They also considered the quantity of damage to the blood cells and stated that in two models, there was a risk of damage to the red blood cells at the final stage of the closure phase. Govindarajan *et al.*¹⁸ conducted a study on the effect of hinges as the leading cause of the clot formation in the closure phase. Two-dimensional geometry, along with the Lagrangian approach, was utilized to follow the platelet path and calculate the shear stress on them along the pass of this area. They reported that a boundary layer separation occurred in a narrow space in the hinges, which resulted in the formation of vortices. Platelets are stuck in this area, and this leads to the process of flocculation. Kuan *et al.*²⁵ attempted to simulate the flow in the valve during the heart cycle and investigated the influence of sinuses and the aortic arch on the micro-flow through the hinges. They reported that high WSS during the diastolic phase is much more than the systolic phase, so blood elements are damaged more significantly in the diastolic phase.

Advancements of systems in recent years have undoubtedly led to more precise simulations resulted in faster valve developments.

On-X heart valves are generally taken into account as a new generation of valves, which are commonly used in recent years; however, the literature lacks information about it. Based on this, Mirkhani *et al.*³⁰

simulated transient blood flow through the On-X mechanical valve in ascending aorta with two-way FSI simulation to investigate fluid flow in all positions of leaflets and detect the areas with the highest shear stresses. They concluded that the On-X valves are able to establish a uniform and relatively laminar flow. After measuring the turbulent and viscous shear stresses, they concluded elevated shear stresses at the inside of the hinges lead to platelet activation and subsequent thrombotic complications. Following the previous work, Hanafizadeh *et al.*¹⁹ tried to investigate the impact of non-Newtonian blood flow with realistic geometry, including coronary arteries. They performed a 3D simulation of a 23-mm On-X valve and blood flow through coronary arteries in the diastolic phase. They investigated the effect of coronary arteries on the hemodynamic efficiency of the valve. The results showed that the presence of BMHV causes a 100% increase in the flow rate in coronary arteries and changes in WSS and, as a result, increasing coronary artery disease. They concluded that ignoring the non-Newtonian characteristics of blood can cause an 80% error in the calculations.

Some researchers worked on investigating the different mathematical activation models. Hedayat *et al.*²⁰ compared the activation of the platelet of a mechanical heart valve (MHV) against BHV (Bio-prosthetic heart valves). They used identical initial hemodynamic and boundary conditions by using three different mathematical activations. Their results indicated that at the beginning of the systole phase, by using MHV instead of BHV, the risk of platelet activation is multiplied. The platelet activation, however, by the bulk flow for the MHV, at the end of the systole phase, was multiple of that for the BHV, and contrary to the previous observations, their results demonstrated that systole phase plays a crucial role in the activation of platelets.

Calcification of the valve is one of the most significant reasons for valve failure and, recently, investigating the impact of calcification of the leaflets on the flow rate has been the focal point of many studies. Calcification and the impact of its severity and distribution on valve leaflets have been investigated by Sturla *et al.*³⁹ The Finite element method was employed in their study utilizing three aortic root models, which had different calcified stenotic aortic valves. *Ex-vivo* assessment of three human aortic valves constituted the basis for the respective calcification patterns. They observed that calcification patterns had effects on implanted stent configuration, stress distribution that was generated on calcium deposits, and high stresses that affect the profile of native aortic valve leaflets. In their study, a relation was proposed between the alteration of the stresses in the native anatomical ele-

ments and prosthetic implant. In another study, leaflet calcification and its effect on flow patterns were investigated by Amindari *et al.*³ They studied the calcification effect by introducing three models of valve material (healthy, calcified, extremely-calcified) using three Young Modulus in a 2D FSI aortic valve case. Their observation revealed that the opening ratios of the valve decreased considerably; when the Young Modulus was changed from healthy to calcified, and it was asserted that calcification led to stenosis. Furthermore, compared to the healthy valve, calcification resulted in a significant rise in average WSS on the leaflets and TPG. By considering the WSS pattern, they showed that the highest WSS was situated at the leaflet tips on all of the occasions.

In previous studies, usually, the effects that vessel wall motions exert on the blood domain have been neglected, while proven to have a significant influence on the simulation results. Bonfanti *et al.*⁸ modeled the type-B aortic dissection (AD) with the deformable vessel wall by using the FSI method and compared the results with a simplified Moving Boundary Method (MBM). They showed that the deformation of the aorta has a sensible impact on the blood flow and, the MBM can capture the wall motion of the flow field with negligible error; in other words, MBM results are approximately in accordance with the results of the FSI simulation. In a recent study, Nowak *et al.*³⁴ developed a numerical model for predicting the blood flow characteristics in the human aorta section. They used the FSI method from the Ansys package for considering the deformation of the vessel wall. They analyzed the differences between rigid and deformable aorta in their study, and the results indicated that the developed model has some impact on the pressure, pressure drop, and wall shear distribution. They claimed that these values are higher in deformable wall conditions both for systole and diastole compare to the rigid wall.

Calcification of the valve is one of the major important reasons for aortic valve replacement, and many types of research have been performed to study the calcification of aortic valve leaflets. However, to the best knowledge of the authors, not enough attention has been paid to calcification of the annulus after implanting the artificial valve. It is worthwhile to mention that calcification of the annulus, which mostly occurs in older people, can proceed up to the beginning of the sinuses. Another scientific gap noticed by the authors is that most of the studies have been performed without considering the effect of aorta deformation while the influence of elasticity of vessel walls and their deformation is noticeable. Hence, the primary goal of this study is to elucidate the effect of aorta deformation on the hemodynamic performance

of BMHVs. In this research, it has been tried to simulate the realistic and the most accurate model for the valve and the deformable aorta in geometry. So, a 3D transient numerical simulation of an On-X medical BMHV size of 23-mm is performed during the accelerating systolic phase considering three different conditions: rigid aorta (referred as *Rigid*), flexible aorta with a healthy annulus (referred as *Flexible*) and flexible aorta with a calcified annulus (referred as *Calcified*).

METHODOLOGY

In this part, the model assembled in silico is presented, and it contains both the structural and fluid domains. For predicting the computational domain, the commercial solver Ansys Workbench 17.2 was utilized. This is due to its ability to analyze the computational domain as well as exchanging data between flow and structural solvers.

Moreover, the numerical procedure and applied boundary conditions are elaborated in order to solve the governing equations.

Geometry Details

As one of the recent most reliable BMHVs, the On-X valve has been proposed in this study. Also, the diameter of the selected model has been considered 23-mm because of its practical application in surgeries. In a realistic situation, the presented valve should be placed over the aortic root. In order to design the geometry of the detailed valve structure, first, the Coordinate Measuring Machine (CMM) is used to provide the cloud point. Figure 1 demonstrates a provided point cloud from the specified BMHV using optical 3D scanning. CMM, as optical measurement



FIGURE 1. Point cloud of the BMHV.

equipment with an approximately 80 μm precision, has been employed.

Next, the final model has been generated through SolidWorks 2017 by utilizing the extracted point clouds and with the help of accessible information presented by the On-X Life Technology Inc. in conjunction with the direct measurements. With the help of these measurements, the leaflet ear and hinge recess surfaces from the point clouds would be smoothed. By merging these data, a realistic 3D model of the BMHV has been developed *via* the SolidWorks 2017 software package. Figure 2 represents the components of the generated valve model. As it is evident, the sewing ring has been eliminated due to being inconsequential to the blood flow pattern that exists within the aortic valve.

It should be noted that the non-symmetric hinge recess is where the leaflet ear is situated. Furthermore, On-X life technology Inc. exclusively presents its designed butterfly shape for hinge recess.³⁵ As can be seen, the leaflet ear and the corresponding hinge have been designed, so that enables the creation of an unswept area at the corners of the hinge. This design results in fluid flow passing the pivot while the risk of generation of flow stagnation is reduced, and as a consequence, lower thrombosis rate is experienced.³⁵

Accordingly, the leaflet of the valve has been considered with 13.5 mm in length, 0.8 mm in thickness, and traveling angle of 40° to 90°.³⁵ Before the closure phase, the leaflets can be opened full 90° according to the “actuated pivot design,” which is the unique feature of On-X valves.³⁵ Figure 3 demonstrates the free rotational leaflets angle where the valve is in its fully closed state. As it is clear, the traveling angle equals 50° because of the symmetric geometry of the leaflets and hinge. It is worthy to mention that the contact exist in the pin section is assumed to be frictionless.

The considered On-X aorta valve is placed over a real ascending aorta model, which including sinuses of Valsalva (thoracic aorta). In order to generate the 3D model, the point cloud of a thoracic aorta has been initially extracted using the segmentation tool provided by computed tomography angiography (CTA) images appertaining to a patient who has been implanted BMHV (CTA images are provided in the Appendix Fig. 24, Fig. 25). By using the extracted point cloud, the curvature centerline corresponding to the thoracic aorta can be achieved. Therefore, the generalized model can be developed using these data along with the available dimensions regarding an average person in previous studies.^{15,29} After generating the geometry of the ascending aorta, the On-X valve is mounted on the aorta. Accordingly, Figure 4 depicts the resulting fluid domain.

In FSI simulations to have accurate data transfer between the fluid domain and solid structure, the

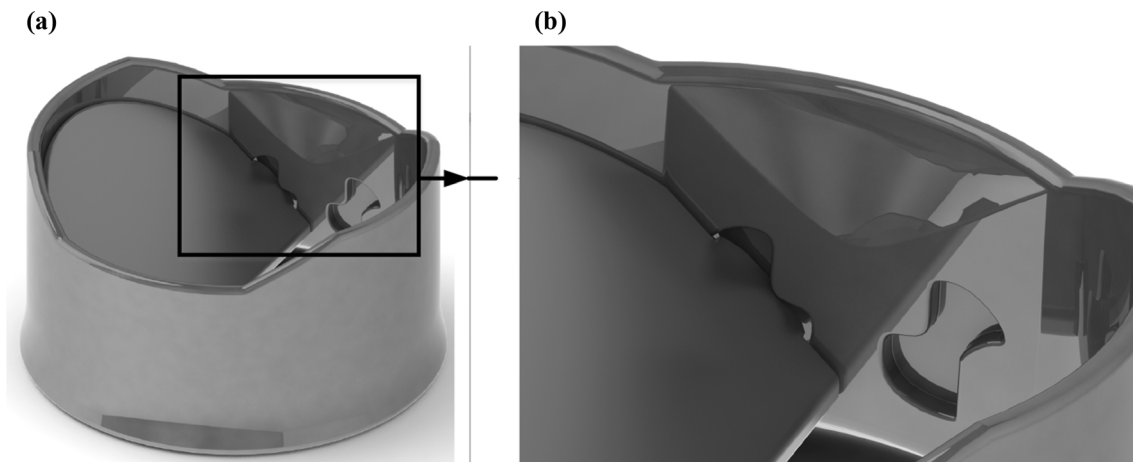


FIGURE 2. (a) On-X heart valve model; (b) magnification of hinge area and leaflet ear.

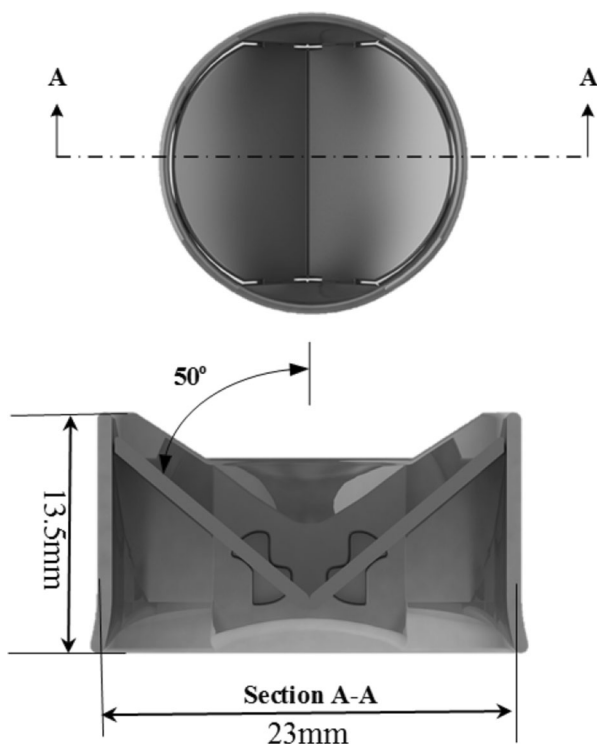


FIGURE 3. Leaflet traveling angle from fully closed to the fully open position.

mesh grid should be fine enough to capture the phenomena occurring in common regions. Moreover, it is highly recommended to use the same mesh grid for fluid and solid domains in the vicinity of FSI interfaces. Therefore, as it is demonstrated in Fig. 5, the mesh grid adjacent to leaflets becomes finer, and it is attempted to generate almost identical mesh grids in FSI interfaces. For capturing the main flow features, it should be guaranteed to have adequate elements in the mentioned gaps, so the fluid domain has been divided into 3,610,146 tetrahedral elements. Also, the mesh

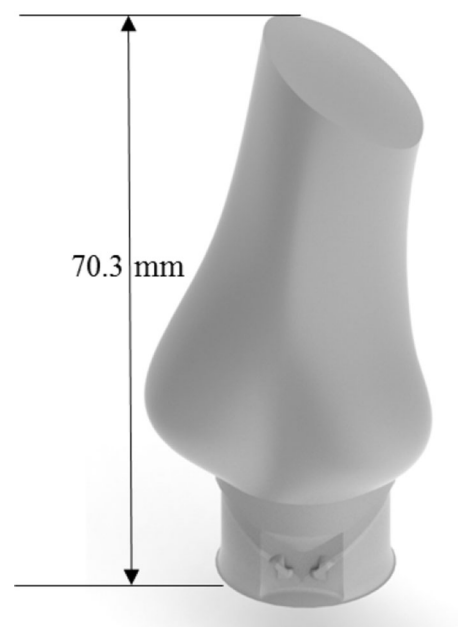


FIGURE 4. Fluid domain inside the ascending aorta with BMHV.

resolution has been altered from $20 \mu\text{m}$ in the gaps to approximately $800 \mu\text{m}$ in the regions far from the vessel wall. The computational grid of the blood flow has been depicted in Fig. 5a. Also, Fig. 5b provides a more detailed demonstration of the mesh closer to leaflets.

The vessel wall is separated into two parts in order to assign different mechanical properties. They are shown in green and blue color as the representation of part A and part B, respectively in Fig. 6. According to this separation, in this study, we have investigated three models: flexible ascending aorta with a healthy annulus (*Flexible*), flexible ascending aorta with a calcified annulus (*Calcified*), and rigid vessel wall (*Rigid*).

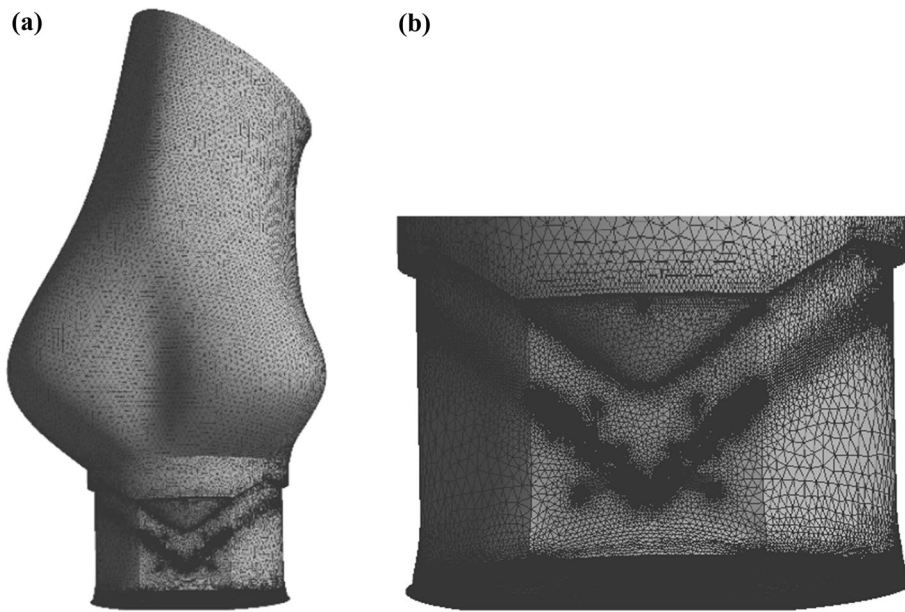


FIGURE 5. Computational mesh (a) fluid domain (b) near the valve region.

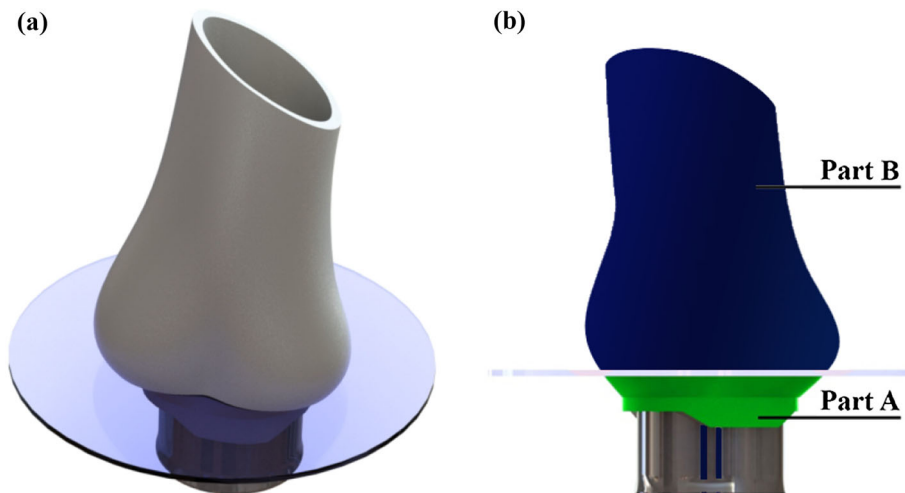


FIGURE 6. (a) 3D schematic of the vessel wall and separation, (b) 2D view of parts A and B of the vessel wall.

Flow and Mechanical Solvers

After assuming the blood flow as an incompressible flow, the blood has been modeled according to the Newtonian shear stress relation, because of high shear rates which is occurred in the blood in the accelerating systole; therefore, the aggregates are destroyed, and the blood cells behave as individuals. Also, the tube diameter and blood hematocrit influence the blood viscosity at a constant strain rate. So, the constant dynamic viscosity of 3.6 cP has been supposed by considering the aorta diameter and the volume fraction for a normal person.³² It should be mention that ALE

formulations were utilized to discretize the computational system.

The following instantaneous Navier–Stokes (NS) equations have been obtained as the governing equations for this case:

The equations containing i and j are presented in tensor notation, which i and $j = 1, 2, 3$.

$$\frac{\partial U_i}{\partial t} + \frac{\partial (U_j - \hat{U}_j) U_i}{\partial x_j} = B_i - \frac{1}{\rho} \frac{\partial P}{\partial x_i} + \frac{1}{\rho} \frac{\partial \tau_{ij}}{\partial x_j} \quad (1)$$

where U , \widehat{U} , ρ , p , μ , and B state the instantaneous velocity vector, interface boundary velocity, density, pressure, dynamic viscosity of the fluid, and the body force, respectively. Besides, the fluid density has been assumed to be 1050 kg/m^3 .

As mentioned before, the turbulence parameters are the critical features of the BMHVs. The Unsteady Reynolds-Averaged Navier–Stokes (URANS) equations are considered to examine these parameters as follows:

$$\rho \frac{\partial u_i}{\partial t} + \rho \frac{\partial (u_j - \widehat{u}_j) u_i}{\partial x_j} = \rho B_i - \frac{\partial P}{\partial x_i} + \frac{\partial}{\partial x_j} \left(\mu \frac{\partial u_i}{\partial x_j} - \overline{u'_i u'_j} \right) \quad (2)$$

where u is the mean velocity and also u' represents the velocity fluctuation in the turbulence field. Hence, the following total stress tensor can be expressed based on the URANS formulation:

$$\overline{\tau}_{ij} = \mu \left(\frac{\partial u_i}{\partial x_j} + \frac{\partial u_j}{\partial x_i} \right) - \overline{\rho u'_i u'_j} \quad (3)$$

In this relation, the second-order tensor $-\overline{\rho u'_i u'_j}$ is the unknown Reynolds stress. The elements of this tensor can be determined through Boussinesq approximation, i.e., turbulent viscosity hypothesis, so they can be linked to the mean flow field. As a result, the final form of total stress is written as:

$$\overline{\tau}_{ij} = \mu \left(\frac{\partial u_i}{\partial x_j} + \frac{\partial u_j}{\partial x_i} \right) + \frac{2}{3} \rho k \delta_{ij} - \mu_t \left(\frac{\partial u_i}{\partial x_j} + \frac{\partial u_j}{\partial x_i} \right) \quad (4)$$

where turbulent or eddy viscosity, μ_t should be determined. To estimate this parameter, since the flow through the aortic valve is transition to turbulent flow, the Realizable $k-\varepsilon$ model is applied.^{21,30} Through the model, the transport equations for turbulent kinetic energy, k , and its dissipation rate, ε , are solved. Using this model, the transient simulation of the hemodynamic performance of BMHVs can carry out, due to its capability for predicting complex flows with significant strain rates such as recirculation and strong pressure gradients. In addition, to satisfy the physics of the blood flow in the near-wall regions, ‘‘Enhanced Wall function,’’ which is one of the sub-models of Realizable $k-\varepsilon$ model was used. The accuracy of this model was investigated by calculating the Y^+ on the aorta wall and leaflets, which is between 3.6 and 6.5.

The eddy or turbulent viscosity is defined as,

$$\mu_t = \rho C_\mu \frac{k^2}{\varepsilon} \quad (5)$$

where variable C_μ is a function of strain and vorticity rate tensors. Now, by considering these relations, the

transport equations can be solved for kinetic energy and its dissipation rate.

As the governing equation for the structure, for the healthy and calcified aortic annulus as well as valve leaflets parts, the following stress tensor can be defined with respect to the linear elastic solids as reported in the literature²²:

$$\sigma_{ij} = \lambda \delta_{ij} e_{kk} + 2G e_{ij} \quad (6)$$

where:

$$\lambda = \frac{Ev}{(1+\nu)(1-2\nu)} G = \frac{E}{2(1+\nu)} \quad (7)$$

In which G is the shear modulus, E is young modulus, e is the displacement gradient tensor, and ν is the Poisson ratio. Considering these relations, the governing equation on the valve leaflets is expressed as,

$$\rho a_j = \frac{\partial \sigma_{ij}}{\partial x_j} + B_j \quad (8)$$

However, for the second part of the vessel wall (part B), according to Karimi’s research,²² with the assumption of deformation for the aorta wall, the Ogden model can be utilized. So, the following stress tensor can be defined concerning the Ogden second-order solids. The Ogden form is based on the principal stretches of the left Cauchy–Green tensor. The strain energy potential is:

$$W = \sum_{i=1}^N \frac{\mu_i}{\alpha_i} \left(\overline{\lambda}_1^{\alpha_i} + \overline{\lambda}_2^{\alpha_i} + \overline{\lambda}_3^{\alpha_i} - 3 \right) + \sum_{i=1}^N \frac{1}{d_k} (J - 1)^{2k} \quad (9)$$

where: W : strain energy potential, $\overline{\lambda}_P (P = 1, 2, 3)$: deviatoric principal stretches, defined as $\overline{\lambda}_P = J^{(-1/3)} \lambda_P$, λ_P = principal stretches of the left Cauchy–Green tensor, J = determinant of the elastic deformation gradient.

As an incompressible elastic linear solid, the material properties of the leaflets have been considered according to the pyrolytic carbon. The vessel wall separates into two parts to assign deferent mechanical behavior (Fig. 6); as previously mentioned, part A represents the annulus part and, part B is the continuation of the ascending aorta, characterized by second-order Ogden model ($N = 2$). The mechanical properties of leaflets, as well as parts A and B in two cases of the healthy and calcified annulus, are reported in Tables 1 and 2.^{10,22}

The fundamental conditions applied to the FSI are the kinematic condition (or displacement compatibility), and the dynamic condition (or traction equilibrium), and the equations are expressed as the followings:

TABLE 1. Linear elastic materials parameters.

Material	Young module (GPa)	Density (kg/m ³)	Poisson's ratio
Leaflets material (pyrolytic carbon)	25	2100	0.3888
Part A healthy annulus	13.8	2100	0.4999
Part A calcified annulus	22.6	2100	0.4999

TABLE 2. Ogden model material parameters.

Parameter	Value
μ_1	25
μ_2	13.8
α_1	22.6
α_2	0.01661
d_1	10^5 (1/Pa)
d_2	10^5 (1/Pa)

$$d_f = d_s \quad (10)$$

$$n \cdot t_f = n \cdot t_s \quad (11)$$

where d_f and d_s are the fluid and solid displacements, respectively, n is the unit normal vector, τ_f , and τ_s are the fluid and solid stresses, respectively.

Ansys coupling FSI technology using the segregated approach for solving the fluid and structure system separately with exchanging data at the fluid-structure interface was utilized in our simulations. In this research, FSI interfaces were assigned at two leaflets and the ascending aorta wall. Since both physics are affected by each other and data is passed in both directions between the fluid and solid models, the two-way coupled FSI using the ALE method was utilized in the simulations. As the boundary displacement, the motion of leaflets and deflection of aorta wall have been transferred to the flow from the transient structural. Therefore, the governing equations have been solved in the updated flow field by employing Fluent. Next, the exerted forces on the solid domain were sent to Ansys mechanical software from Fluent. Subsequently, the governing equations on the valve leaflets and aorta wall are solved. Figure 7 shows the flow chart of the system coupling and data transition in every time step.

In each FSI iteration, the iterative process between CFD and FEM solver (data exchange between Ansys Fluent and Ansys mechanical), will continue until the converged solution is reached.

In the Fluent section, the dynamic mesh considering smoothing/remeshing was enabled to reform and regenerate the mesh following moving boundaries. The

smoothing setting is to control the damping of the springs, and we choose 0 as “spring constant factor” to let boundary node displacements have more influence on the motion of the interior nodes. To avoid convergence problems, we selected “local cell” and “local face” from remeshing box for this simulation. The details of dynamic mesh formulation are presented in ANSYS Fluent User's Guide17.2.⁴ Besides, the details of “solutions methods” implemented in Ansys Fluent are presented in the Appendix Table 7.

By considering a heart rate of 75 beats/min and a cardiac output of 6.1 L/min, the transient simulation has been presented with a total period of 180 ms for the accelerating systole. The fixed time-stepping method with 0.5 ms time step has been chosen in Fluent, and in the system coupling, the maximum number of iterations per time step was set to 10 to enhance the temporal resolution. In this simulation the accelerating phase was studied, and it was proven that in this period, the flow is fairly repeatable from cycle to cycle,¹¹ so only one cycle was considered in our simulation.

For the current simulation, Fig. 8 demonstrates the corresponding cardiac cycle, including the valve opening. As the inlet boundary condition, the physiologic flow rate by the red line has been set for the fluid domain, i.e., the uniform time-dependent aortic flow rate was set as left ventricular outflow. Also, the pressure outlet boundary condition (end of the modeled ascending aorta) has been assigned by the aortic pressure wave represented by the blue line in Fig. 8. Indeed, this pressure wave refers to the pressure of aortic blood. Finally, at the initial moment, a fully closed position has been considered for the leaflets.

It is worth stating that a series of grid-independence tests have been carried out using different mesh sizes for the *Flexible* model. Through these tests, one of the foremost parameters of the valve performance, the gradient of transvalvular pressure at peak systole, was investigated for different cell numbers. In Fig. 9, the variation of this parameter for the cell numbers in the range of 1.3×10^6 to 8×10^6 is depicted. It can be observed that the domain with 3.6×10^6 cell numbers is appropriate to predict the valve performance with lower than 2.6% error.

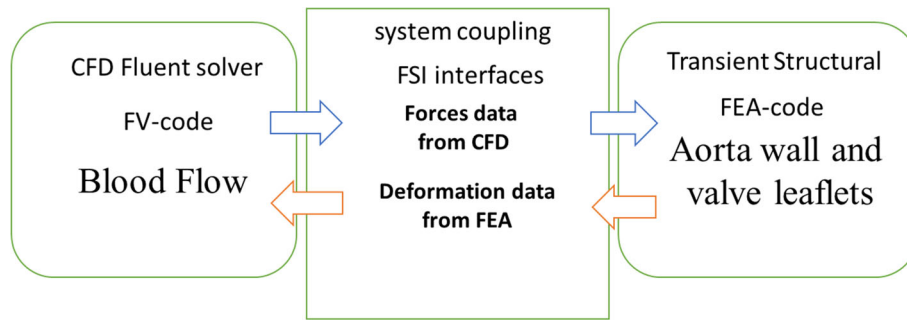


FIGURE 7. Flow chart of data exchanging in each FSI iteration.

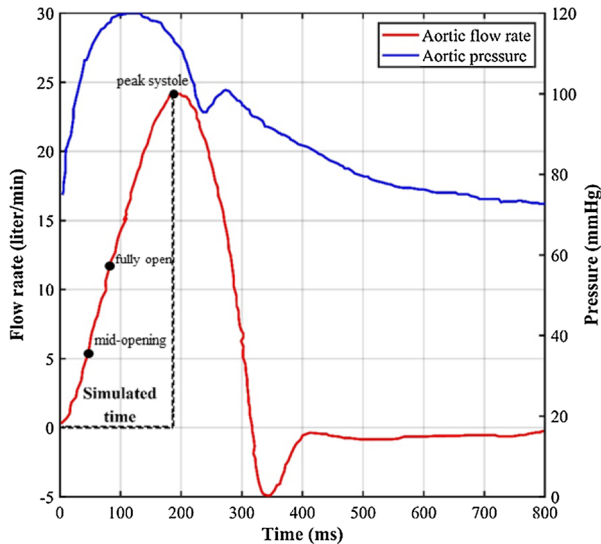


FIGURE 8. Physiologic flow and pressure waves of the ascending aorta.

Similarly, to perform the mesh study on the structural domain, the effect of mesh element number on relative area changes of the plane II in Fig. 12(b) was investigated at $t = 40$ ms. The plan was considered in the sinus region which has more changes in comparison to the other parts of the ascending aorta. It was shown in Fig. 9(b) that a mesh size comprising 823,789 tetrahedral and pyramid elements has less than 1.6% error.

It is worthy to mention that the analyses consumed around 400 h to simulate *Flexible* and *Calcified* models and 250 h for *Rigid* aorta case on 40 processors with 3.5 GHz frequency and 32 Gb of Ram.

RESULTS AND DISCUSSION

The results of the FSI simulation are presented in what follows. In the first part, flow characteristics were calculated in the flow domain under the assumption of the *Flexible* model. In the second part, the effects of utilizing various material models on the characteristics of the flow and the dynamics of the leaflets are studied. Results are tried to be presented for three main time points: mid-opening ($t = 0.04$ s), open leaflets ($t = 0.08$ s) and peak systole ($t = 0.18$ s).

Flow Characteristics in Flexible Model

In order to evaluate the valve performance, measuring the pressure gradient in the safe range ensures that the heart is not exposed to excessive external work and possible hypertrophy. So, immediately after aortic valve replacement, it is calculated by using echo-cardiography. In Fig. 10 the location of the points, in which the TPG was calculated is demonstrated. The TPG is calculated as the pressure gradient between points (a) and (b), which are demonstrated in Fig. 10 ($TPG = P_a - P_b$). Palatianos *et al.*³⁶ reported from clinical values that the TPG at the peak of systole is 12.3 ± 6.2 mmHg. According to the result from the *Flexible* model, this parameter was revealed to be 14.53 mmHg, which is in the experimental range.

To investigate the performance of the valve, analyzing other factors than TPG like turbulence intensity, flow pattern, velocity profile, and shear stress are essential and need to be discussed in total flow, especially in the regions that are at the risk of platelet activation and hemolysis such as the hinges, sinuses, and the downstream flow.

Laminar flow is physiologically more desirable as the turbulence in the flow leads to higher energy loss, and therefore, more pressure is imposed on the heart.

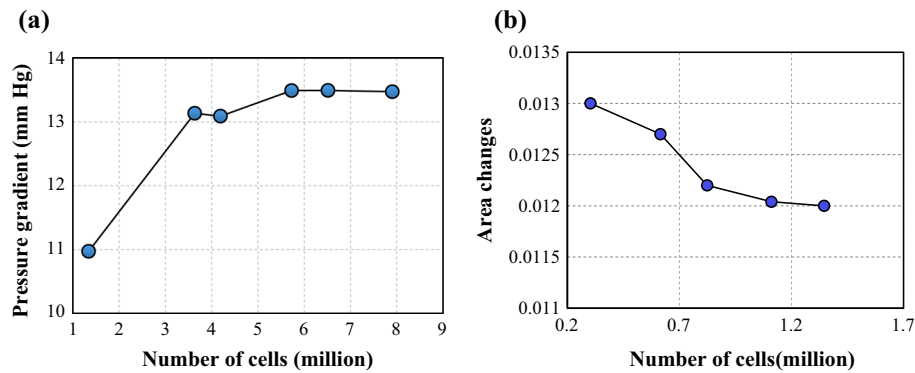


FIGURE 9. Grid independency study (a) fluid (transvalvular pressure gradient vs. element numbers) and (b) structure (Area changes at $t = 40$ ms vs. element numbers).

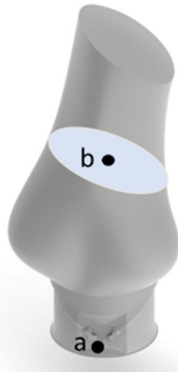


FIGURE 10. (a) Left ventricular outflow, (b) aortic valve outflow.

Thus, the valve's geometry should be designed in a way that the resulted blood flow pattern is in physiologically preferable conditions.

First, for a better understanding of the flow and movement of the valve, the streamlines are shown in Fig. 11, which are colored according to the magnitude of velocity, for mid-opening Fig. 11(a) and fully open Fig. 11(b) states for the Flexible model.

The On-X valves are able to form a comparably uniform flow pattern due to their flared inlet. As it is shown, the flow initially sticks to the wall, but after the opening of the valve and the increase of velocity in the side jets, the flow is separated from the wall in the sinus region, and the fluid vorticities are created. These vortices in the mechanical valve increase the stagnation time of the particles in blood, which can lead to hemolysis and activation of the platelets. The formation of vortices in the sinus is due to the implant of the valve in the annulus and the distance of valve from sinuses area. This flow pattern is in perfect agreement with the results of the Akutsu,² which states that in the On-X valve at early systole there is less diffusive flow, and the flow resembles jet-like pattern at the downstream of the valve. For a better view of the triple jet and its variation throughout the vessel, Fig. 12(a) demonstrates the contour of

velocity magnitude at fully open states in a mid-plane crossing the valve. As it is known, due to the difference between the geometry of the mechanical valve and the natural valve, the flow through the On-X valve is converted into triple-jet. As the blood moves inside the ascending aorta, the structure of triple-jet fades and forms the approximately uniform flow that is expected to be generated.² In Fig. 12(b), the velocity contours are plotted at the three parallel plates with various distances from the inlet. As it is clearly illustrated, in the fully-open state mode, the valve angle is less than 90° due to the fact that the three orifices in the valve create two nozzles shaped and a diffuser shaped regions and consequently, the geometry of the central jet leads to a slight increase in pressure in the central orifice. An increase in the pressure balance of the flow leads the leaflets to fluctuate around 85° . Figure 13 shows the velocity profile on three lines that are made by intersecting the mid-plane with per-versely described parallel planes. As already mentioned, the triple jet flow at the beginning of the valve turns into an almost uniform flow at the beginning of the arc. Figure 13 profiles are displayed at $t = 80$ ms (i.e., fully open state).

Another critical factor in the valve is the blood velocity and its direction in the vicinity of the hinge. The microflow in this area is the crucial factor in starting thrombus and blood cell damage. Figure 14 illustrates the velocity contours in the hinges region in a parallel plane to the hinge floor in $300 \mu\text{m}$ distance. For more clarification of the flow pattern, the velocity vectors in the region are also presented. As can be seen, lateral flow is formed in the hinge area that plays the most important role in the development of stagnant points and vortices. However, two major streams found within the hinge region are perceived to function optimal pivot cleansing, which is the unique feature of the On-X valve differentiating it from other types of BMHVs.

It is of great importance to study the formation of turbulent fluctuations and eddies in the systole phase

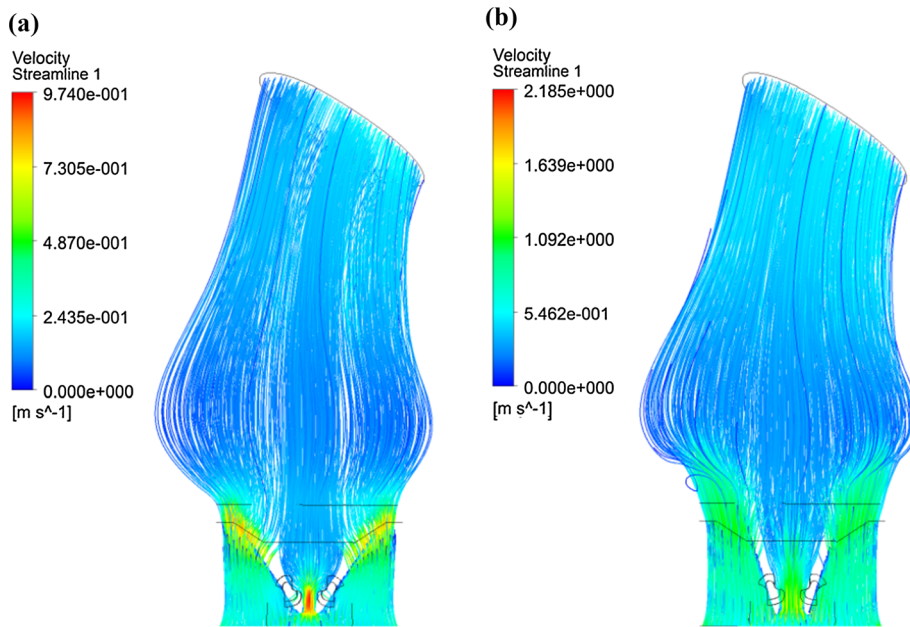


FIGURE 11. Blood streamlines in ascending aorta during the opening process from the side view at (a) mid-opening and (b) fully open position of the leaflets.

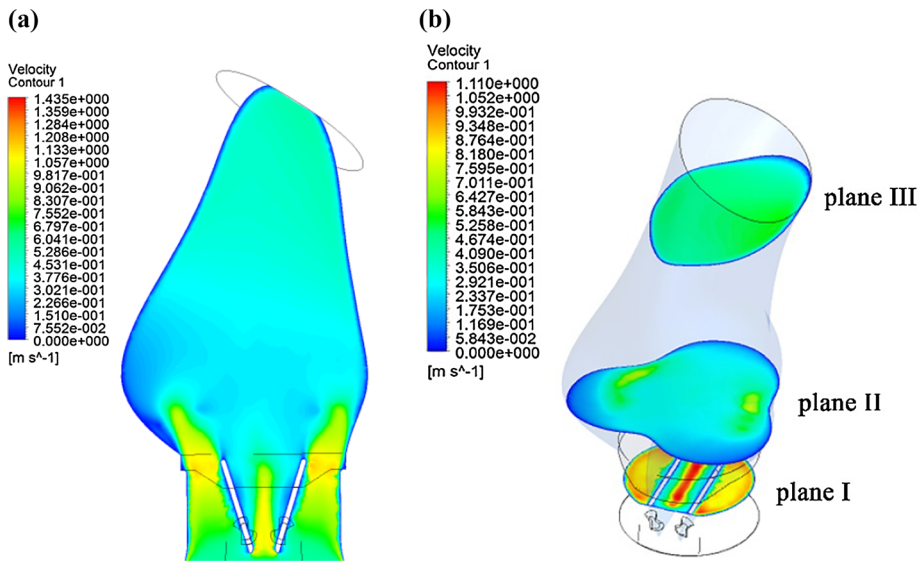


FIGURE 12. Velocity contours (a) at the mid-plane (b) at the three planes with different distances from the valve.

as they can adversely degrade the valve performance by increasing the risk of platelet activation. Thus, the analyzing of the turbulence intensity during the flow passage of the vessel is essential. For this, in Fig. 15, TKE are shown at three parallel planes at different distances from the flow input. As can be seen, in accelerating phase, in the plane 1, shear layers in leaflets vicinity are manifested as the TKE, and by going to the downstream the shear layers are fading, and approximately uniform flow is obtained in the ascending aorta.¹¹

As previously stated, thromboembolism and long term anticoagulant therapy are the most important source of difficulties in mechanical valves, and the activation of platelets is considered by measuring the amount of shear stress in areas with the highest values.

The viscous stress in tensor notation is obtained from the following relationships,

$$\tau_{ij} = 2\mu D_{ij} - \mu_t \left(\frac{\partial u_i}{\partial x_j} + \frac{\partial u_j}{\partial x_i} \right) \quad (12)$$

$$D_{ij} = \frac{1}{2} \left(\frac{\partial u_i}{\partial x_j} + \frac{\partial u_j}{\partial x_i} \right) \quad (13)$$

and the tensor of turbulent stress is obtained based on: $(\tau_{ij})_t = 2\mu_t D_{ij}$.

The non-diagonal components of this stress tensor are shear stresses that should be measured across the entire domain of fluid. As previously stated, their peak is taken place in the region of the hinge due to the passing of the blood flow from the small area. The maximum turbulence and viscous shear stresses in three planes parallel to the floor wall of the hinge are considered in the Table 3.

From a molecular standpoint, both viscous shear stress and turbulent shear stress can be associated with collisions behind, although they have distinct mechanisms. So, it is necessary to measure both of the stresses to assure that they have not surpassed the damage levels. As the results show, stresses in the hinge

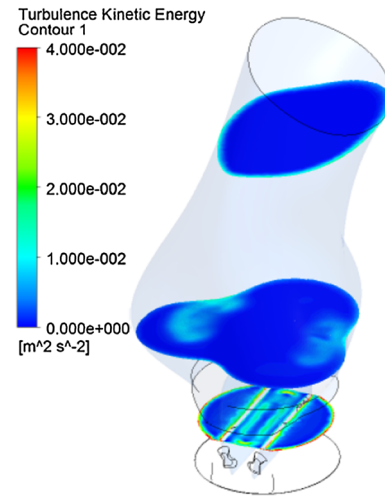


FIGURE 15. Contours of turbulent kinetic energy at three planes with different distances from the valve.

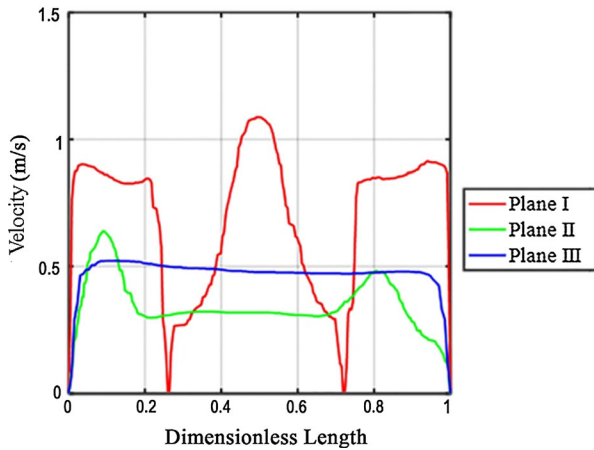


FIGURE 13. Variations of velocity profile with distance from the valve.

TABLE 3. Maximum shear stress at three critical planes.

	Viscous	Turbulent
Maximum shear stress (Pa) (plane 1)		
τ_{xy}	49.12	23.54
τ_{xz}	46.16	23.96
τ_{yz}	106.43	35.84
Maximum shear stress (Pa) (plane 2)		
τ_{xy}	54.05	35.23
τ_{xz}	55.44	18.43
τ_{yz}	59.74	28.57
Maximum shear stress (Pa) (plane 3)		
τ_{xy}	58.99	58.42
τ_{xz}	58.63	17.88
τ_{yz}	52.70	26.03

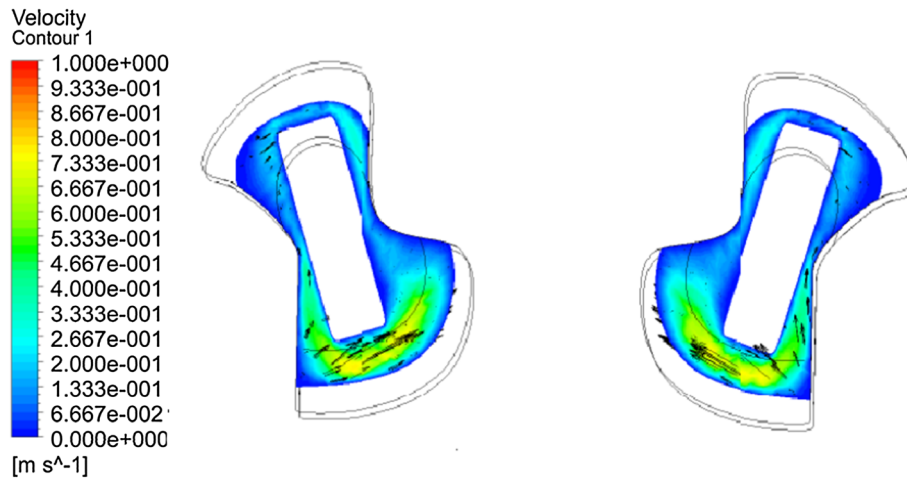


FIGURE 14. Velocity contours and vectors inside the hinge recess at a plane with a distance of 300 μm from the hinge floor.

region can cause platelet activation and hemolysis. Moreover, as our results indicate, and Tullio *et al.*¹² concluded, these two parameters are in the same order and have an equal effect on hemolysis and platelet activation.

Another parameter that should be checked is vorticity, which is the curl of velocity, as it can entrap the blood cells. The recirculating zones increase the exposure time of the blood flow; thus, it is recommended to be prevented in these valves. The analysis of the recirculation zones helps us to determine the areas that are at the risk of thromboembolism. Based on a critical value for vorticity introduced by Morbiducci,³¹ the region with vorticity of greater than 800 1/s is in the risk to damage blood, which is demonstrated at mid-opening and fully open in Fig. 16.

The vortical structure generally passes through the peripheral gap space, and by opening the valve, it moves toward downstream.

The valve housing is another criteria to analyze the possibility of thrombus initiation in the valve vicinity. Kuan reported that WSS on the valve housing should be approximately 400 Pa for hemolysis, but in the presence of platelet activation, the wall shear stress of 10 Pa is adequate for triggering this detrimental process.²⁵ WSS distribution on the valve housing during the accelerating systole is shown in Fig. 17. Although the inlet flared orifice produces approximately uniform flow, this geometry results in increasing wall shear stress, even more than 400 Pa because of the effect of the flow on the surface in the housing area.

For predicting the cavitation process, investigating the dynamic of the leaflet, such as leaflet tip velocity, is essential.¹² The study was done by Lee²⁷ shown that most of the cavitation bubbles were observed at the

leaflet tip, and there is a correlational relationship between the leaflet velocities and cavitation intensity.²⁷ Therefore, the maximum angular velocity of On-X leaflets was measured that for the *Flexible* model is 11.6221 rad/s, which is lower than the ones reported in conventional BMHVs and more closely resemble a trileaflet valve.²⁸ This can be attributed to two main reasons. First, the traveling angle of the current BMHV, which is about 40°, is lower than that of other BMHVs. Next, accurate simulation achieved from utilizing two-way FSI coupled solver and exact modeling of the gaps in the geometry. Thus, an increase in the resistant forces is observed, and as a result, the maximum angular velocity of the leaflets is reduced.

Leaflet normalized angle in the opening process is represented in Fig. 18. In this figure, the normalized opening angle of this simulation is compared with the experimental and numerical results in the literature.^{11,38,40} As it can be observed, all numerical simulation results can acceptably predict the opening trend, while there is a delay in predicting the opening angle. This delay was considered acceptable concerning the opening phase time-lapse of 50 ms.³³ However, the results obtained in the current study are closer to experimental data in comparison to previous 3D work.

Influence of Vessel Wall Material

In this section, the influential parameters in hemodynamics of blood flow in three models of the vessel wall are compared, and it is shown that the vessel wall flexibility, as well as annulus calcification, have sensible influences on blood flow critical parameters like velocity, vorticity, TKE, and even TPG. The streamlines of the blood flow in the mid-opening and fully

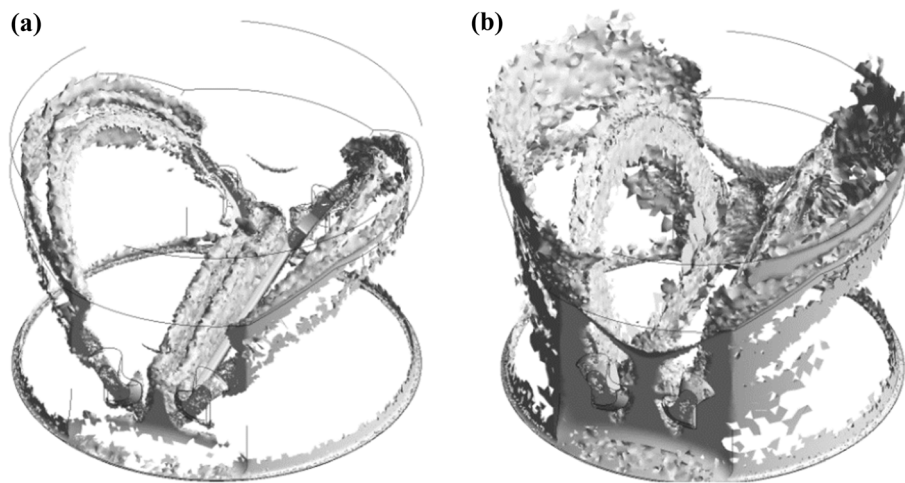


FIGURE 16. High vorticity volume through the fluid domain at (a) mid-opening state and (b) fully open state.

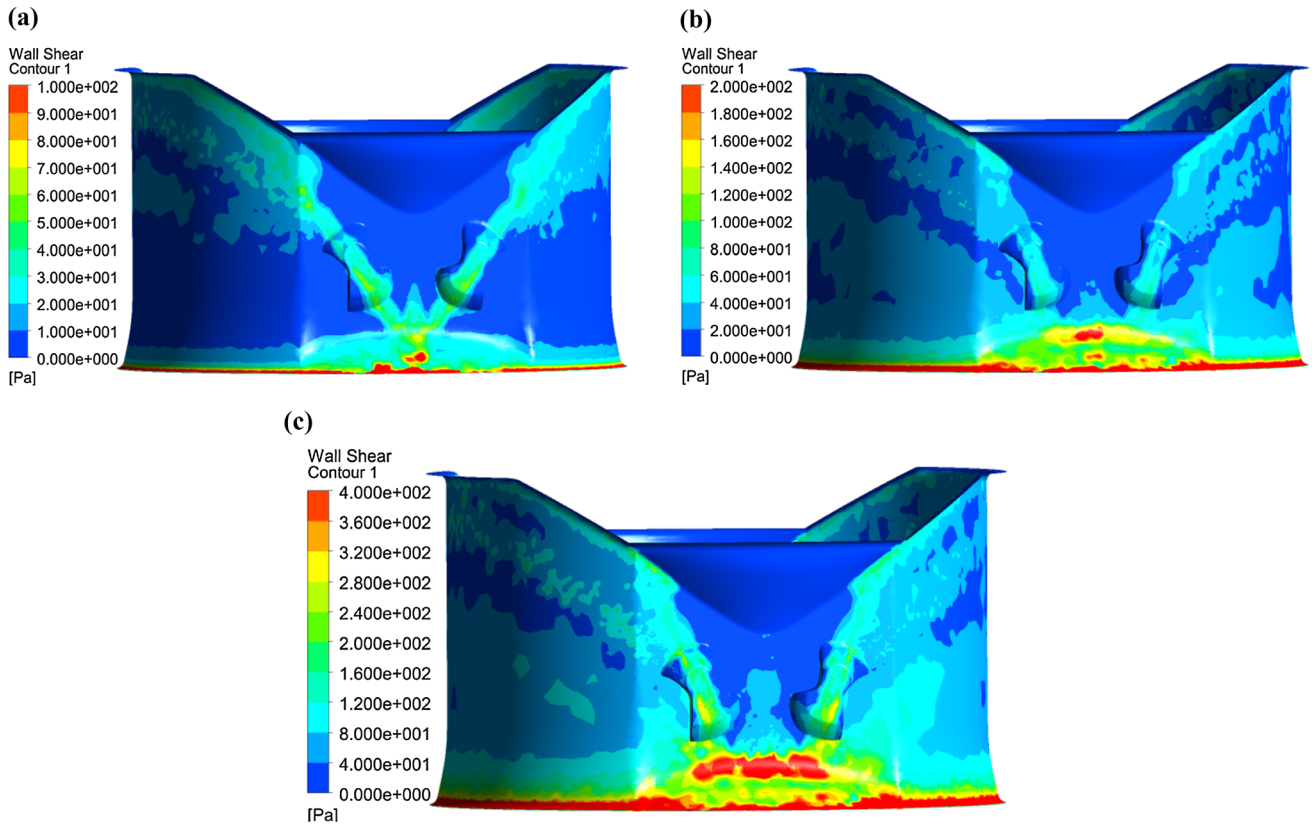


FIGURE 17. Distribution of the wall shear stress on the housing during the accelerating systole for three time points for (a) mid-opening, (b) open leaflets and (c) peak systole.

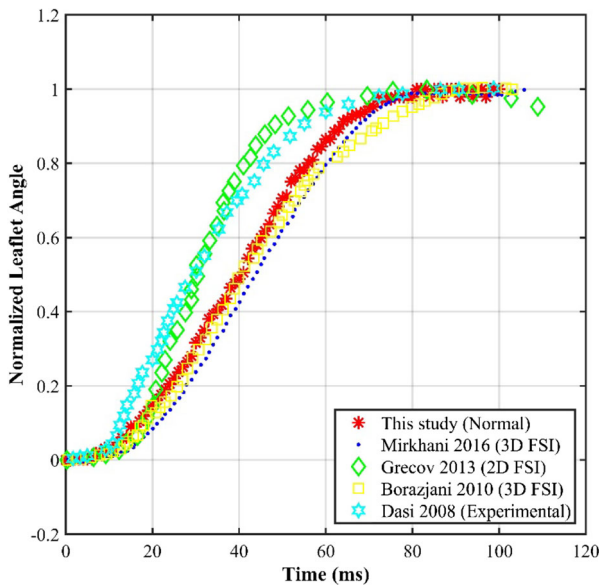


FIGURE 18. Normalized leaflet angle comparison.

open state for three models are shown in Fig. 19 and Fig. 20 respectively.

As clearly depicted in Fig. 19 and Fig. 20, the most significant differences were observed in the vicinity of the leaflets and central jet up to the beginning of the

sinuses. During leaflets opening, It was found that except the little region in the central jet and just during the time between 67 ms up to fully open state (80 ms), the velocities in the *Flexible* and the *Calcified* models are always less than the *Rigid* model which is due to the peripheral expanding of the vessel wall in flexible and calcified models. It can be argued that in the mid-opening state (40 ms), the vessel wall deformation has tangible effects on the velocity because the effects of the velocity and traction boundary conditions are instantly transmitted to the vessel wall in the *Flexible* and the *Calcified* models where the structure is assumed hyperelastic. These effects are pronounced in velocity at both beginnings of the valve and the systole phase. So, the *Flexible* model predicts the lower value of the maximum of velocity compared with the *Rigid* model by 6% at $t = 40$ ms, because of the peripheral expanding of the vessel wall. Moreover, it can be interpreted as a little part of initial kinetic energy in the *Flexible*, and the *Calcified* models are used to initiate vessel deformation. The *Calcified* model shows characteristics between the *Rigid* and the *Flexible* models and more similar to the *Rigid* model due to featuring a higher elastic modulus in the annulus part where the maximum velocity occurs, so it yields to 4% higher maximum velocity than the *Flexible*. At fully open

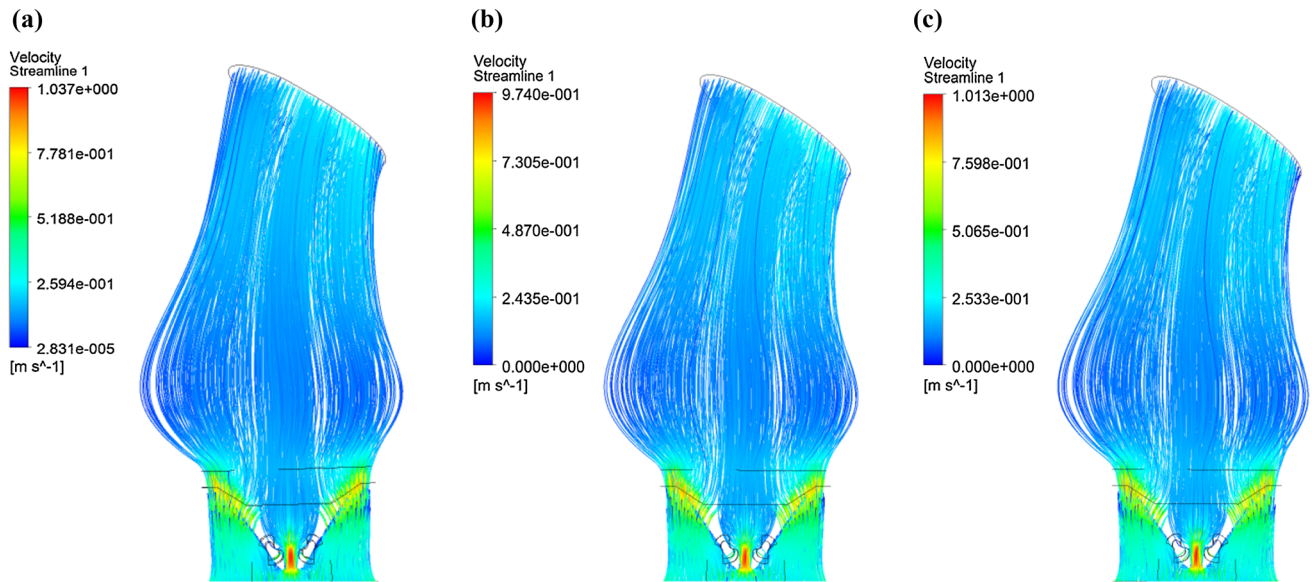


FIGURE 19. Blood streamlines in ascending aorta during the opening process from the side view at mid-opening for three models of (a) rigid, (b) flexible, and (c) calcified.

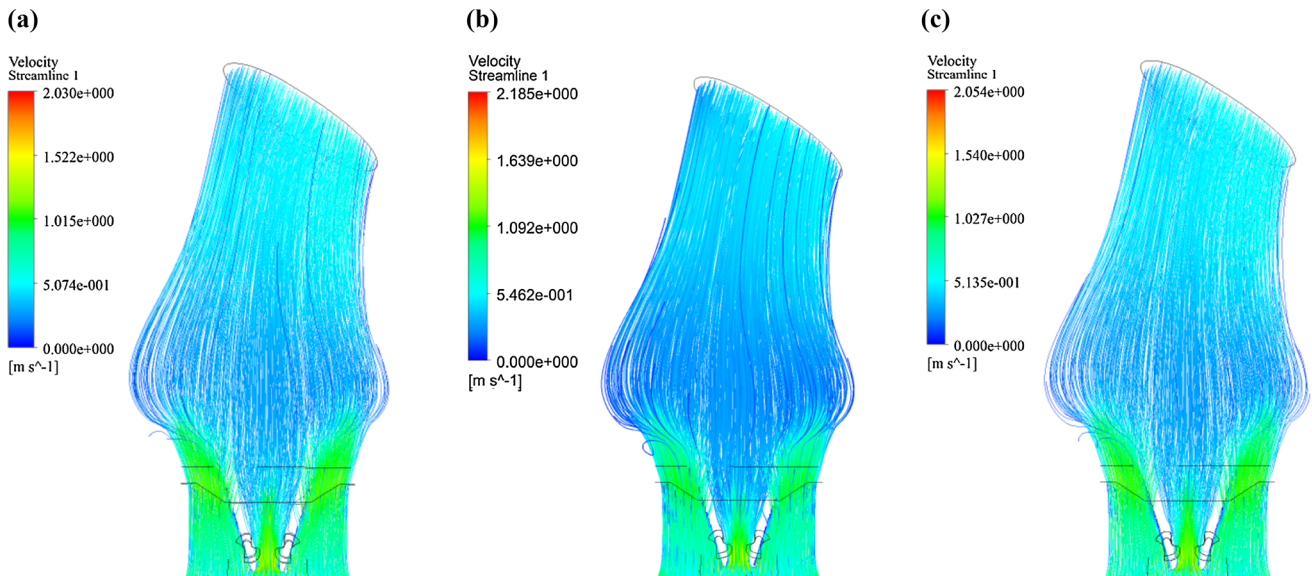


FIGURE 20. Blood streamlines in ascending aorta during the opening process from the side view at fully open for three models of (a) rigid, (b) flexible, and (c) calcified.

state ($t = 80$ ms), these differences become more noticeable, and especially in the central jet and even sinuses areas, because changes are transmitted to the upper surface over time. In the central jet area, the *Flexible* model predicts the higher value of maximum velocity than the *Rigid* model by 7% at $t = 80$ ms, since the velocity in beside jets are decreasing, and the total area in the valve housing is constant. However, after housing of the valve, the velocities in the *Rigid* model are slightly more than the *Flexible* one during leaflets opening process. By changing the model from the *Flexible* to the *Calcified*, the maximum velocity is

decreased by 6%. As it is clear, after the sinuses area, the differences are faded, and in the downstream, the velocity profiles become all alike, which can be correlated to the changes of cross-sectional areas that are shown in three planes in Fig. 21.

Figure 21 shows the surface changes to the initial level for the *Flexible* and the *Calcified* models in three planes parallel to inlet (Plane I is located just after the housing of the valve and plane II and plane III were described in Fig. 12(b)). As it can be seen, the maximum surface area changes for the *Flexible* and the *Calcified* models up to fully open state are approxi-

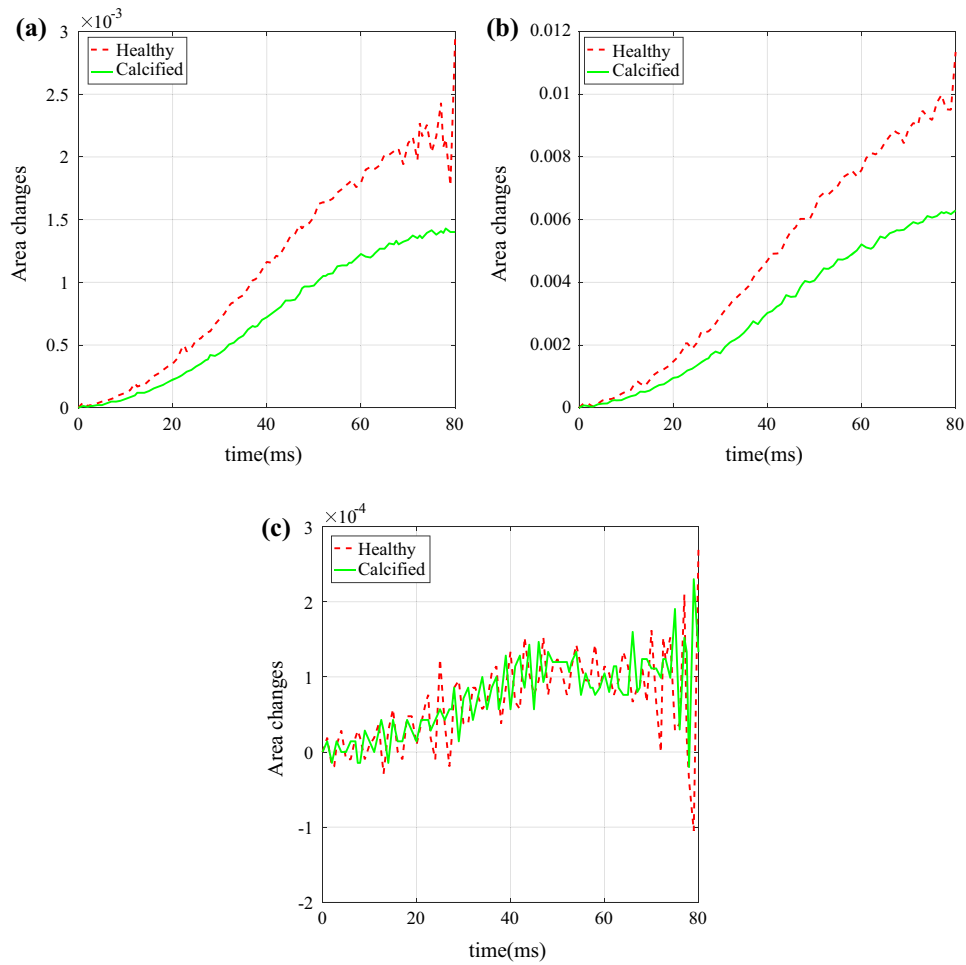


FIGURE 21. The surface areas changes to the initial areas over time up to fully open state in the Flexible and the Calcified models in three planes, (a) plane I, (b) plane II, and (c) plane III.

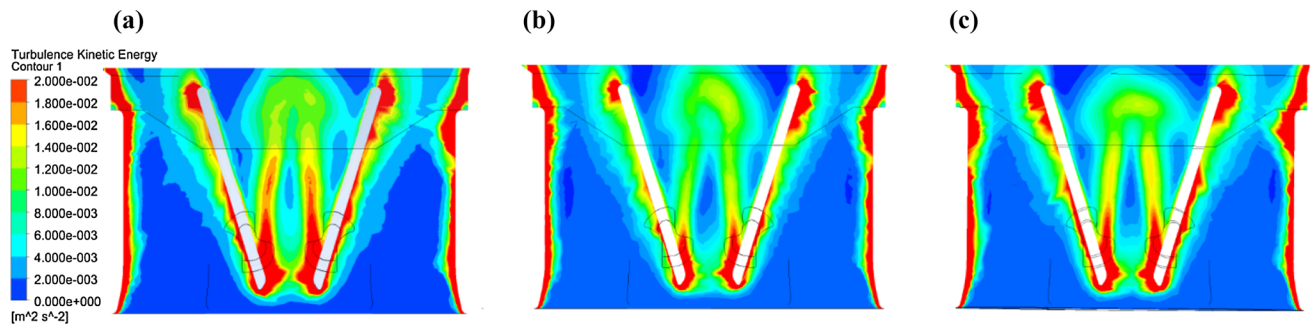


FIGURE 22. Contours of turbulent kinetic energy at fully open state in ascending aorta at the mid-plane (housing section) for three models of (a) rigid, (b) flexible, and (c) calcified.

mately 0.0025 and 0.0015 respectively in plane I, while in the sinuses plane (plane II), the values are 0.01 and 0.006 respectively. Nevertheless, in the beginning of the arch (plane III), the surface area changes are about 0.0003 and 0.0002 for the *Flexible* and the *Calcified* models, respectively, which are negligible and, therefore, velocities profiles approximately coincide with each other. This is due to the combined effect of the

viscous damping of flow and the fact that kinetic energy is absorbed by the walls during the acceleration phase in the form of potential energy to expand the walls. But the vessel wall cross-sectional areas have higher frequency oscillations in the deformation in both *Flexible* and *Calcified* models in the downstream (plane 3).

As stated before, the TKE of the blood flow is very important. In Fig. 22, the influence of the vessel wall deformation on the turbulent kinetic energy in three models in a fully open state is depicted.

As it can be seen, the local TKE in the *Flexible* model in some regions of the central jet is less than that of the *Rigid* one up to 20% in the fully open state and, it is because of the more velocity magnitude in the central jet in the *Rigid* model. For a more detailed examination, a point in the central jet of the valve domain is selected, and correspondingly the TKE values for three models are reported in Table 4 at the fully open state.

In the *Calcified* model, due to the elastic modules applied to the material, the material has more stiffness and therefore behaves more like the *Rigid* model. The numerical results indicate that in the central jet region, which the most significant TKE differences between models occur, the *Calcified* model shows 5% higher TKE than the healthy annulus (*Flexible* model) at point 1.

Vorticity is a substantial quantity that indicates the creation and intensity of the recirculating zones in the blood flow and, consequently, the platelet activation.

TABLE 4. Turbulent kinetic energy at point 1 at the fully open state (80 ms).

	Rigid	Flexible	Calcified
Turbulent kinetic energy (J/Kg)	0.01135	0.009387	0.009821

Figure 23 depicts the influence of the vessel wall deformation and annulus calcification on the vorticity in three models in a fully open state.

As it is illustrated in Fig. 23, in the fully open state, larger vortical structures develop in the central jet for the *Flexible* model and it can be correlated with a higher velocity gradient in this region in the *Flexible* model. Additionally, the vorticity given by the *Calcified* model is less than the *Flexible* model. For a more detailed examination, a point in the domain is selected, and correspondingly the TKE values for three models are reported at fully-open state in Table 5.

As it is measured at point 1, in the central jet region, the vorticity of the *Flexible* model is about 10% higher compared with the *Rigid* model, while this value for the *Calcified* model is about 5% less than that of the *Rigid* model.

Finally, the values of TPG are presented in Table 6.

Table 6 shows the results associated with transvalvular pressure gradient at three-time state for the three models. The reported values are all reasonably acceptable and within the measured experimental range.³⁶ The TPG in the *Flexible* model is higher than the measured value in the *Rigid* model. The greater

TABLE 5. Vorticity at point 1 at the fully open state of the leaflets (80 ms).

	Rigid	Flexible	Calcified
Vorticity (1/s)	87.8	98.13	83.28

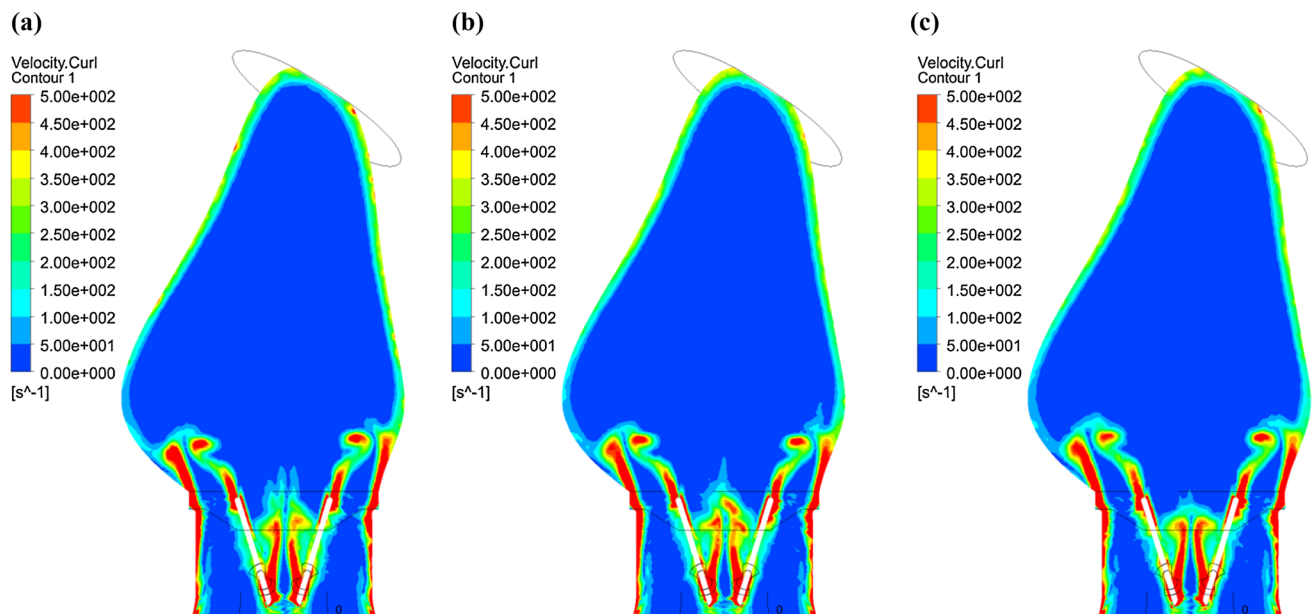


FIGURE 23. Contours of vorticity at fully open state in ascending aorta at the mid-plane for three models of (a) rigid, (b) flexible, and (c) calcified.

TABLE 6. Pressure gradient through the valve.

	Time state (ms)	Rigid	Flexible	Calcified
Pressure gradient (mmHg)	40	4.976	5.220	5.009
	80	7.524	8.320	7.534
	180	13.41	14.53	13.95

TPG refers to the vessel deformation. In other words, in systole phase up to 80 ms, in the *Flexible* model, because of wall elasticity, more amount of flow pressure energy is absorbed by the aorta wall. In the *Calcified* model, aorta wall is less deformed due to the Young modulus; consequently, the TPG is also lower compared with the *Flexible* model.

CONCLUSION

The main focus of this article was to investigate the complex flow field characteristics in the new generation of BMHVs with the flexible vessel wall. By taking into account the wall flexibility as well as utilizing the FSI method, it is expected to achieve the results of valve implementation with desirable accuracy. It was shown that the transvalvular pressure gradient of On-X valves is in the safe level and is in agreement with the literature. Numerical simulations indicate that, in accelerating systole, On-X valves are capable of producing jet-like and approximately uniform flow in the downstream. It was shown that by using the On-X valve, large scale eddies along with turbulences produced by the valve are faded before reaching the aortic arch. As it was mentioned, the vortices and turbulent eddies started from the vicinity of the valve leaflets go to the downstream of the fluid domain as the time goes on. Moreover, the maximum turbulent and viscous shear stresses in the fluid domain were evaluated, and it was found that the blood flow around the hinge region is in the danger of hemolysis and platelet activation and subsequently thromboembolism. Another critical re-

gion was found to be the sinuses region wherein observed vorticities indicate recirculating zones and, consequently, the high risk of thromboembolism. Results from considering the viscous and turbulent shear stress indicate that the accelerating systole phase has a leading role in the activation of platelets. To investigate the cavitation, the tip velocity was calculated, and it was discovered that the valve is not prone to cavitation. The next key finding of this work was proving that the vessel wall deformation influences the fluid flow parameters of the central jet region. By changing the model from the *Rigid* to the *Flexible* up to fully open state, fluid velocity in some regions is decreased up to 6%, and in the case of Calcified annulus of the aorta, the local velocity is decreased 4% compared with the *Flexible* model which leads to more discrepancies in TKE and vorticity. Moreover, the TPG was also affected by the vessel wall deformation, and in the peak systole time, by changing the model from *Rigid* to the *Flexible* the TPG is increased 8.5%, and with Calcified annulus, the TPG is decreased 4.2% compared with the *Flexible* model. Therefore, similar to vessel wall deformation, considering the probable annulus calcification after valve replacement is also essential.

APPENDIX

See Fig. 24, Fig.25 and Table 7.

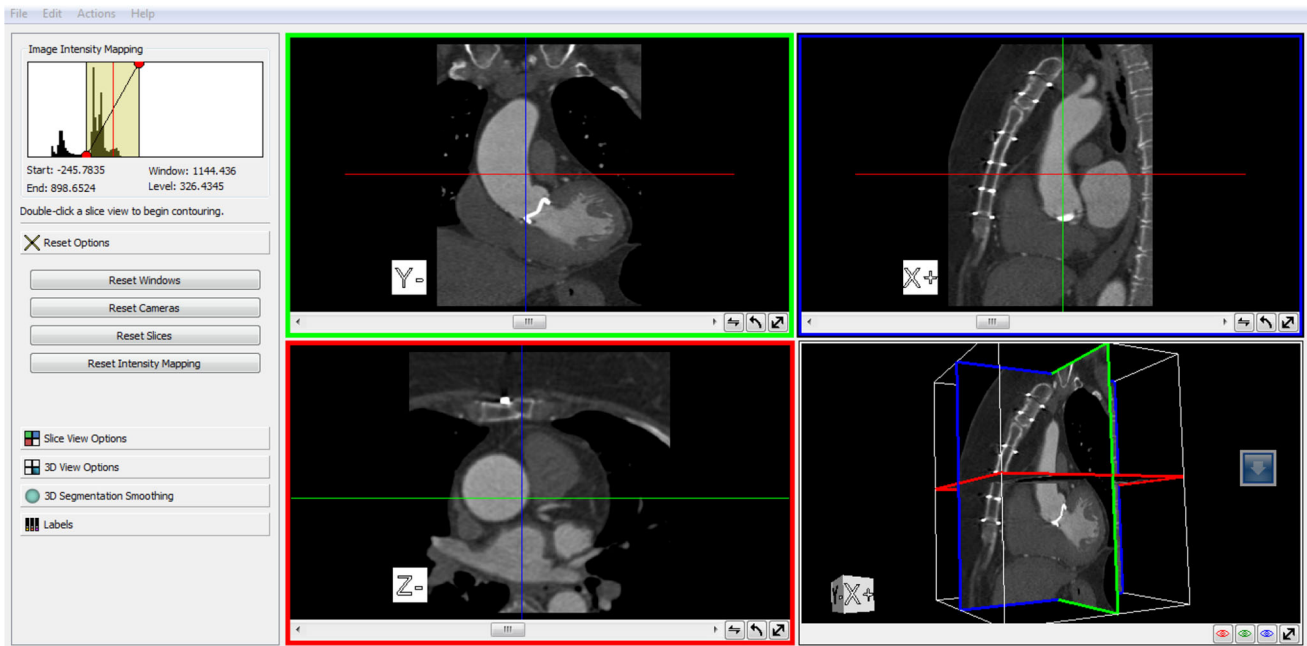


FIGURE 24. CTA images of the person with aortic On-X valve.

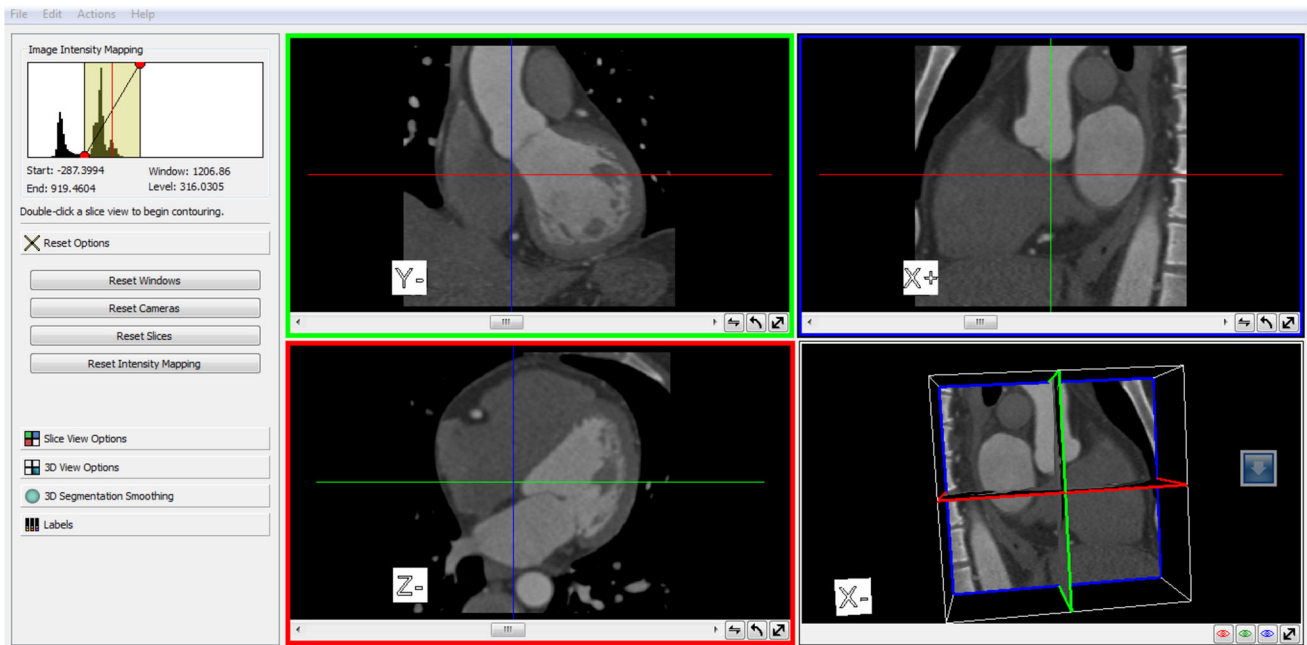


FIGURE 25. CTA images of the person with a healthy valve.

TABLE 7. Solution methods in fluent (Spatial discretization).

Solution methods	Pressure velocity coupling	Simple
	Gradient discretization	Least squares cell based
	Pressure discretization	Standard
	Momentum discretization	Second-order
	Turbulent kinetic energy	First-order upwind
	Turbulent discretization rate	First-order upwind

REFERENCES

- ¹Akutsu, T., and D. Higuchi. Effect of the mechanical prosthetic mono-and bileaflet heart valve orientation on the flow field inside the simulated ventricle. *J. Artif. Organs* 3(2):126–135, 2000.
- ²Akutsu, T., and A. Matsumoto. Influence of three mechanical bileaflet prosthetic valve designs on the three-dimensional flow field inside a simulated aorta. *J. Artif. Organs* 13(4):207–217, 2010.
- ³Amindari, A., L. Saltik, K. Kirkkopru, M. Yacoub, and H. C. Yalcin. Assessment of calcified aortic valve leaflet deformations and blood flow dynamics using fluid-structure interaction modeling. *Inform. Med. Unlocked* 9:191–199, 2017.
- ⁴ANSYS, A. ANSYS Fluent User's Guide, 17.2. Canonsburg: ANSYS, 2016.
- ⁵Bang, J. S., S. M. Yoo, and C. N. Kim. Characteristics of pulsatile blood flow through the curved bileaflet mechanical heart valve installed in two different types of blood vessels: velocity and pressure of blood flow. *ASAIO J.* 52(3):234–242, 2006.
- ⁶Beckmann, A., A. K. Funkat, J. Lewandowski, M. Frie, M. Ernst, K. Hekmat, W. Schiller, J. F. Gummert, and W. Harringer. German heart surgery report 2016: the annual updated registry of the German Society for Thoracic and Cardiovascular Surgery. *Thorac. Cardiovasc. Surg.* 65(07):505–518, 2017.
- ⁷Bluestein, D., E. Rambod, and M. Gharib. Vortex shedding as a mechanism for free emboli formation in mechanical heart valves. *J. Biomech. Eng.* 122(2):125–134, 2000.
- ⁸Bonfanti, M., S. Balabani, M. Alimohammadi, O. Agu, S. Homer-Vanniasinkam, and V. Díaz-Zuccarini. A simplified method to account for wall motion in patient-specific blood flow simulations of aortic dissection: Comparison with fluid-structure interaction. *Med. Eng. Phys.* 58:72–79, 2018.
- ⁹Cheng, R., Y. G. Lai, and K. B. Chandran. Three-dimensional fluid-structure interaction simulation of bileaflet mechanical heart valve flow dynamics. *Ann. Biomed. Eng.* 32(11):1471–1483, 2004.
- ¹⁰Chien, H. L., B. W. Huang, and J. H. Kuang. The Ogden model for coronary artery mechanical behaviors. *Life Sci.* 8(4):430–437, 2011.
- ¹¹Dasi, L. P., L. Ge, H. A. Simon, F. Sotiropoulos, and A. P. Yoganathan. Vorticity dynamics of a bileaflet mechanical heart valve in an axisymmetric aorta. *Phys. Fluids* 19(6):067105, 2007.
- ¹²De Tullio, M. D., A. Cristallo, E. Balaras, and R. Verzicco. Direct numerical simulation of the pulsatile flow through an aortic bileaflet mechanical heart valve. *J. Fluid Mech.* 622:259–290, 2009.
- ¹³Dumont, K., J. M. A. Stijnen, J. Vierendeels, F. N. Van De Vosse, and P. R. Verdonck. Validation of a fluid-structure interaction model of a heart valve using the dynamic Karimi method in fluent. *Comput Methods Biomech. Biomed. Eng.* 7(3):139–146, 2004.
- ¹⁴Dumont, K., J. Vierendeels, R. Kaminsky, G. Van Nooten, P. Verdonck, and D. Bluestein. Comparison of the hemodynamic and thrombogenic performance of two bileaflet mechanical heart valves using a CFD/FSI model. *J. Biomech. Eng.* 129(4):558–565, 2007.
- ¹⁵Evangelista, A., F. A. Flachskampf, R. Erbel, F. Antonini-Canterin, C. Vlachopoulos, G. Rocchi, R. Sicari, P. Nihoyannopoulos, J. Zamorano, Document Reviewers, and M. Pepi. Echocardiography in aortic diseases: EAE recommendations for clinical practice. *Eur. J. Echocardiogr.* 11(8):645–658, 2010.
- ¹⁶Ge, L., L. P. Dasi, F. Sotiropoulos, and A. P. Yoganathan. Characterization of hemodynamic forces induced by mechanical heart valves: Reynolds vs. viscous stresses. *Ann. Biomed. Eng.* 36(2):276–297, 2008.
- ¹⁷Ge, L., H. L. Leo, F. Sotiropoulos, and A. P. Yoganathan. Flow in a mechanical bileaflet heart valve at laminar and near-peak systole flow rates: CFD simulations and experiments. *J. Biomech. Eng.* 127(5):782–797, 2005.
- ¹⁸Govindarajan, V., H. S. Udaykumar, and K. B. Chandran. Two-dimensional simulation of flow and platelet dynamics in the hinge region of a mechanical heart valve. *J. Biomech. Eng.* 131(3):031002, 2009.
- ¹⁹Hanafizadeh, P., N. Mirkhani, M. R. Davoudi, M. Masouminia, and K. Sadeghy. Non-Newtonian blood flow simulation of diastolic phase in bileaflet mechanical heart valve implanted in a realistic aortic root containing coronary arteries. *Artif. Organs* 40(10):E179–E191, 2016.
- ²⁰Hedayat, M., H. Asgharzadeh, and I. Borazjani. Platelet activation of mechanical versus bioprosthetic heart valves during systole. *J. Biomech.* 56:111–116, 2017.
- ²¹Johansen, P. Mechanical heart valve cavitation. *Expert Rev. Med. Devices* 1(1):95–104, 2004.
- ²²Karimi, A., M. Navidbakhsh, M. Alizadeh, and A. Shojaei. A comparative study on the mechanical properties of the umbilical vein and umbilical artery under uniaxial loading. *Artery Res.* 8(2):51–56, 2014.
- ²³King, M. J., J. Corden, T. David, and J. Fisher. A three-dimensional, time-dependent analysis of flow through a bileaflet mechanical heart valve: comparison of experimental and numerical results. *J. Biomech.* 29(5):609–618, 1996.
- ²⁴King, M. J., T. David, and J. Fisher. An initial parametric study on fluid flow through bileaflet mechanical heart valves using computational fluid dynamics. *Proc. Inst. Mech. Eng.* 208(2):63–72, 1994.
- ²⁵Kuan, Y. H., F. Kabinejadian, V. T. Nguyen, B. Su, A. P. Yoganathan, and H. L. Leo. Comparison of hinge micro-flow fields of bileaflet mechanical heart valves implanted in

- different sinus shape and downstream geometry. *Comput. Methods biomech. Biomed. Eng.* 18(16):1785–1796, 2015.
- ²⁶Kwon, Y. J. Numerical analysis for the structural strength comparison of St. Jude Medical and Edwards MIRA bileaflet mechanical heart valve prostheses. *J. Mech. Sci. Technol.* 24(2):461–469, 2010.
- ²⁷Lee, H., A. Homma, and Y. Taenaka. Hydrodynamic characteristics of bileaflet mechanical heart valves in an artificial heart: cavitation and closing velocity. *Artif. Organs* 31(7):532–537, 2007.
- ²⁸Li, C. P., and P. C. Lu. Numerical comparison of the closing dynamics of a new trileaflet and a bileaflet mechanical aortic heart valve. *J. Artif. Organs* 15(4):364–374, 2012.
- ²⁹Mao, S. S., N. Ahmadi, B. Shah, D. Beckmann, A. Chen, L. Ngo, F. R. Flores, Y. lin Gao, and M. J. Budoff. Normal thoracic aorta diameter on cardiac computed tomography in healthy asymptomatic adults: impact of age and gender. *Acad. Radiol.* 15(7):827–834, 2008.
- ³⁰Mirkhani, N., M. R. Davoudi, P. Hanafizadeh, D. Javidi, and N. Saffarian. On-X heart valve prosthesis: numerical simulation of hemodynamic performance in accelerating systole. *Cardiovasc. Eng. Technol.* 7(3):223–237, 2016.
- ³¹Morbiducci, U., R. Ponzini, M. Nobili, D. Massai, F. M. Montevicchi, D. Bluestein, and A. Redaelli. Blood damage safety of prosthetic heart valves. Shear-induced platelet activation and local flow dynamics: a fluid-structure interaction approach. *J. Biomech.* 42(12):1952–1960, 2009.
- ³²Nichols, W. W. Vascular impedance. McDonald's blood flow in arteries: theoretical, experimental and clinical principles. Baco Raton: CRC Press, pp. 243–283, 1998.
- ³³Nobili, M. A. T. T. E. O., G. Passoni, and A. Redaelli. Two fluid-structure approaches for 3D simulation of St. Jude Medical bileaflet valve opening. *J. Appl. Biomater. Biomech.* 5(1):49–59, 2007.
- ³⁴Nowak, M., B. Melka, M. Rojczyk, M. Gracka, A. J. Nowak, A. Golda, W. P. Adamczyk, B. Isaac, R. A. Bialecki, and Z. Ostrowski. The protocol for using elastic wall model in modeling blood flow within human artery. *Eur. J. Mech. B* 77:273–280, 2019.
- ³⁵On-X Prosthetic Heart Valve Design and Features - On-X Life Technologies, Inc. <https://www.onxlti.com/medical-professionals/on-x-prosthetic-heart-valve-design-and-features>.
- ³⁶Palatianos, G. M., A. M. Laczkovics, P. Simon, J. L. Pomar, D. E. Birnbaum, H. H. Greve, and A. Haverich. Multicentered European study on safety and effectiveness of the On-X prosthetic heart valve: intermediate follow-up. *Ann. Thorac. Surg.* 83(1):40–46, 2007.
- ³⁷Siu, S. C., and C. K. Silversides. Bicuspid aortic valve disease. *J. Am. Coll. Cardiol.* 55(25):2789–2800, 2010.
- ³⁸Sotiropoulos, F., and I. Borazjani. A review of state-of-the-art numerical methods for simulating flow through mechanical heart valves. *Med. Biol. Eng. Comput.* 47(3):245–256, 2009.
- ³⁹Sturla, F., M. Ronzoni, M. Vitali, A. Dimasi, R. Vismara, G. Preston-Maher, G. Burriesci, E. Votta, and A. Redaelli. Impact of different aortic valve calcification patterns on the outcome of transcatheter aortic valve implantation: a finite element study. *J. Biomech.* 49(12):2520–2530, 2016.
- ⁴⁰Yeh, H. H., D. Grecov, and S. Karri. Computational modelling of bileaflet mechanical valves using fluid-structure interaction approach. *J. Med. Biol. Eng.* 34(5):482–486, 2014.
- ⁴¹Yun, B. M., J. Wu, H. A. Simon, S. Arjunon, F. Sotiropoulos, C. K. Aidun, and A. P. Yoganathan. A numerical investigation of blood damage in the hinge area of aortic bileaflet mechanical heart valves during the leakage phase. *Ann. Biomed. Eng.* 40(7):1468–1485, 2012.
- ⁴²Zakerzadeh, R., M. C. Hsu, and M. S. Sacks. Computational methods for the aortic heart valve and its replacements. *Expert Rev. Med. Devices* 14(11):849–866, 2017.

Publisher's Note Springer Nature remains neutral with regard to jurisdictional claims in published maps and institutional affiliations.